APPLIED PHYSICS LETTERS **104**, 243103 (2014)

Trapping and aerogelation of nanoparticles in negative gravity hydrocarbon flames

Rajan K. Chakrabarty,[1,2,a)] Igor V. Novosselov,[3,4] Nicholas D. Beres,[2] Hans Moosmüller,[2] Christopher M. Sorensen,[5] and Christopher B. Stipe[6]

[1]*Department of Energy, Environmental & Chemical Engineering, Washington University in St. Louis, St. Louis, Missouri 63130, USA*
[2]*Laboratory for Aerosol Science, Spectroscopy, and Optics, Desert Research Institute, Nevada System of Higher Education, Reno, Nevada 89512, USA*
[3]*Department of Mechanical Engineering, University of Washington, Seattle, Washington 98195, USA*
[4]*Enertechnix Inc., Maple Valley, Washington 98068, USA*
[5]*Condensed Matter Laboratory, Department of Physics, Kansas State University, Manhattan, Kansas 66506, USA*
[6]*TSI Incorporated, 500 Cardigan Rd, Shoreview, Minnesota 55126, USA*

(Received 12 May 2014; accepted 2 June 2014; published online 17 June 2014)

We report the experimental realization of continuous carbon aerogel production using a flame aerosol reactor by operating it in negative gravity ($-g$; up-side-down configuration). Buoyancy opposes the fuel and air flow forces in $-g$, which eliminates convectional outflow of nanoparticles from the flame and traps them in a distinctive non-tipping, flicker-free, cylindrical flame body, where they grow to millimeter-size aerogel particles and gravitationally fall out. Computational fluid dynamics simulations show that a closed-loop recirculation zone is set up in $-g$ flames, which reduces the time to gel for nanoparticles by $\approx 10^6$ s, compared to positive gravity (upward rising) flames. Our results open up new possibilities of one-step gas-phase synthesis of a wide variety of aerogels on an industrial scale. [http://dx.doi.org/10.1063/1.4884057]

Aerogels are volume spanning, semirigid networks of solid nanoparticles (NPs).[1] Owing to their unique material properties such as ultralow density and high surface area,[2] these mesoporous materials have found extensive applications ranging from catching space dusts to purifying air and water supplies.[2,3] However, aerogel synthesis via the sol-gel process is non-continuous and requires supercritical point drying, hence is time-consuming and expensive.[1] This has prevented their mass production and widespread application.[2] Cost-effective and continuous synthesis routes using gas-phase flame aerosol reactors (FARs),[4] which have been widely adopted by industries for production of nanostructured materials,[5] are yet to be demonstrated as viable options for producing aerogels.

In the gas-phase, aerogels form from a dispersion of NPs via the process of irreversible diffusion-limited cluster aggregation (DLCA).[6] DLCA starts out in the limit of spatially uncorrelated binary cluster collisions (cluster dilute regime[6]) to partially relieve the system of its non-equilibrium condition[7] and leads to formation of fractal NP clusters with fractal dimension ≈1.8. This continues until the cluster volume fraction (f_{clus})—the ratio of cluster separation to size—increases to the point where clusters no longer encounter each other in a spatially uncorrelated manner, that is, the cluster-dense regime.[6] In this regime, when the f_{clus} reaches unity, the clusters jam together to form a gel. The phase of high f_{clus} is an absolute necessary condition for gelation to occur. The time for a gel to form, t_{gel}, can be approximated as

$$t_{gel} \approx \frac{4}{3}\pi K^{-1} a^3 f_v^{-2.5}, \tag{1}$$

where a is the radius of the basic NP repeating unit (or monomer) constituting a cluster, f_v is the monomer volume fraction, and K is the aggregation kernel, which specifies the cluster aggregation rate.[8] The approximate Eq. (1) is both simplistic and instructive in laying down the strong functional dependence of t_{gel} on f_v and a.

Conventional sol-gel routes allow sufficient residence time t_{res} (several hours to days) for NPs in a solution to reach threshold t_{gel}.[1] On the contrary, NPs experience t_{res} on the order of submilliseconds[4] in an upward rising ($+g$; positive gravity) FAR. In such rapid kinetics conditions, an initial monomer $f_v \geq 10^{-4}$ is needed to yield a t_{gel} that is shorter than t_{res}.[6] Such high f_v values have been observed to exist locally in the annular region of a heavily sooting $+g$ diffusion flame's tip.[9] However, the high shear stress accompanying the buoyant tip challenges the structural stability of a gel-like cluster network, and tears it apart.[10] The fragmented NP clusters, after exiting the tip, encounter a high dilution zone in the flame's over-fire region, where high f_v conditions are impossible to achieve. Thus, unsustainable cluster-dense f_v conditions, very low t_{res}, and buoyancy-induced instabilities of a $+g$ flame have rendered FARs unsuitable for gel synthesis.

In this Letter, we demonstrate that for FARs operated in an up-side-down ($-g$; negative gravity) configuration, the necessary gelation conditions of cluster-dense f_v and enhanced t_{res} are steadily maintained in a large cross-sectional area of the flame body. A "U" shaped, closed but non-tipping zero-acceleration plane of stagnation is created

[a)]Author to whom correspondence should be addressed. Electronic mail: rajan.chakrabarty@gmail.com

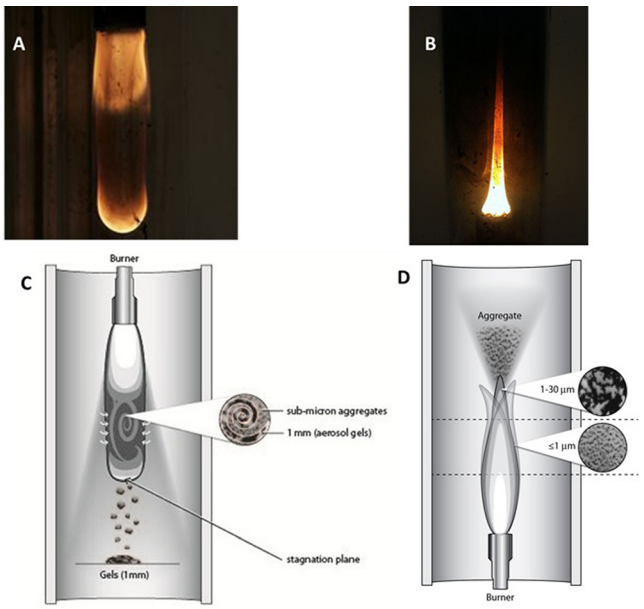

FIG. 1. Gravitational effects on emitted particle morphology from flames. (a) and (b) Photographs of our diffusion FAR operated in downward ($-g$) and upward ($+g$) configurations under same flow conditions. The fuel used was acetylene. The dark region in the middle of the −g flame body is the recirculation zone, from where gel particles fall out. (c) and (d) Schematic of particle formation in these flame systems. In $-g$ flames, cluster-dilute particles get trapped in a deeply metastable recirculation zone. This zone is formed due to the opposing effects of buoyancy on fuel-air flow forces. With time, the particles cross-over to cluster-dense conditions and get structurally arrested to form gel particles. In contrast, a $+g$ flame buoyantly convects out cluster-dilute particles from the flame body. While these particles encounter (for a fraction of a second) a cluster-dense zone near the tip of the flame, the shear stress associated with the flickering flame front does not allow gel formation.

by the effect of buoyancy opposing the fuel and air flow fields[10,11] (Fig. 1). This plane is stable and non-flickering, and traps NP clusters from convectionally flowing out of the flame body. As a result, the trapped clusters experience sufficient $t_{res} > t_{gel}$, which enable them to cross-over to the cluster-dense regime and gel. The clusters gel continuously in the flame and fall out gravitationally once they grow above a threshold gel size.

We operated a basic co-flow, Burke-Schumann arrangement diffusion FAR[10] in both $-g$ and $+g$ configurations to systematically study the differences in emitted NP cluster properties. The flame was housed in a 48.3 cm long and 4.75 cm diameter quartz tube. Hydrocarbon fuel flowed through a 1.9-cm diameter inner tube, while combustion air was injected into the annular region between the fuel jet and the outer quartz tube. We fed the burner with two hydrocarbon fuels of varying threshold soot index (TSI),[12] namely, ethylene and acetylene. The flow rates of fuel and air were varied to tune the net fuel-to-air equivalence ratio (φ).[13] For ethylene, we varied the fuel flow rates between 1.2 and 2.0 l min^{-1} and the co-flow air rates between 16.5 and 17.5 l min^{-1}. For acetylene, we fixed the air flow rate at 105 l min^{-1} and varied the fuel flow rates between 0.5 and 0.8 l min^{-1}. Under these flow conditions, φ varied between 0.92–1.54 and 0.12–0.2 for ethylene and acetylene, respectively. We observed the $-g$ flame morphologies to be significantly longer, wider, and cylindrical in shape, compared to $+g$ flames operated under same flow conditions (Fig. 1). Gel particles were gravitationally settling out from flame bodies and were collected on petri dishes placed below the flame for structural analysis. The quantity of gel production increased with increasing φ and fuel TSI.

Figure 2 shows electron microscopy (EM) and optical microscopy images for acetylene aerosol gel particles. Here, we

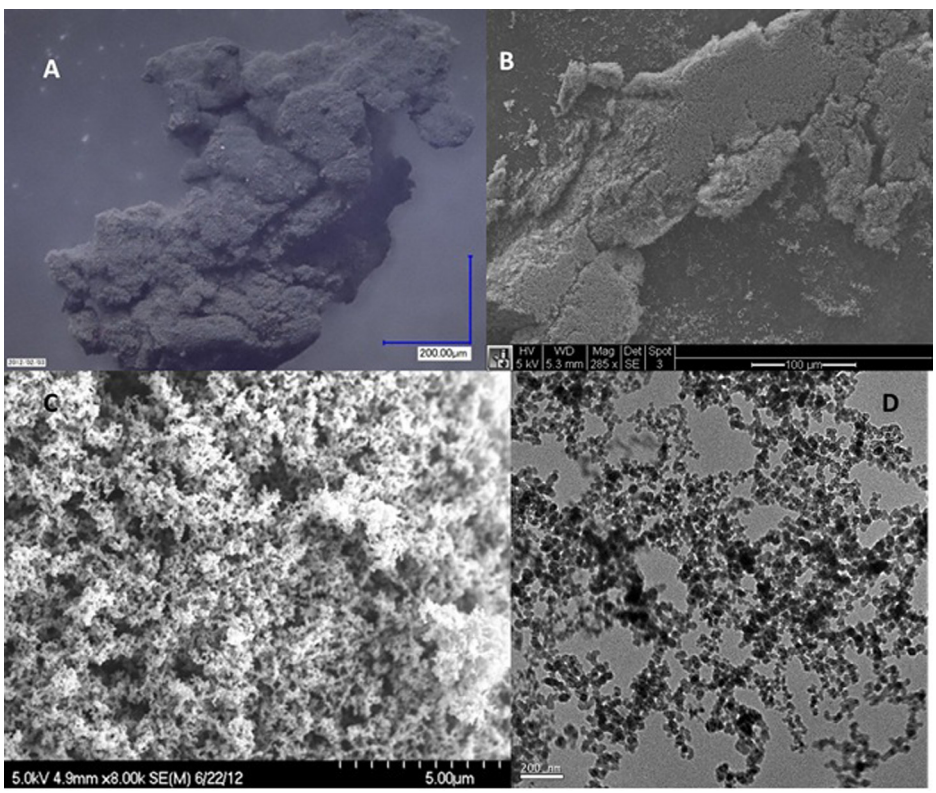

FIG. 2. Morphology of aerosol gel clusters in different length-scales. (a) and (b) Optical and scanning electron microscopy (SEM) pictures of millimeter-size acetylene gel particles produced by our $-g$ flame aerosol reactor. (c) and (d) SEM and transmission electron microscopy images of the microscopic structure of gel particles. These images suggest that the particles are mesoporous and consist of ≈20-nm diameter monomers.

specifically chose to present results from our acetylene combustion experiments. Acetylene is a fuel widely used in industries and research laboratories for manufacturing carbon black powder. Our burner produced a maximum of 5 g h^{-1} of acetylene gel particles. Figures 2(a)–2(d) graphically demonstrate that a macroscopic aerosol gel particle, greater than a millimeter in size, forms from the aggregation of radius $a \approx 10$ nm carbon NPs (monomers). In contrast, the average size of an aggregate emitted from a $+g$ FAR is sub-micron (≤ 1 μm) with $a \approx 20$ nm.[14] The EM pictures show that the aerosol gels are ramified fractal structures with pores trapped inside. The specific surface areas (SSAs) and surface porosity of these gel particles were determined using the Brunauer-Emmett-Teller analysis technique with nitrogen gas as an adsorbate.[15] The gel particles were found to have a mean SSA of 208 m^2/g, which is about four times higher than that of soot aggregates generated by $+g$ FARs.[15] These particles were found to have a specific mesopore volume of 0.24 cm^3/g for a mean pore size of 1.7 nm. We determined the gel (effective) density of the particles, by measuring the mass of a known volume of the sample, to be as low as 4.5 mg/cm^3.

We performed detailed computational fluid dynamics simulations for an axisymmetric laminar acetylene-air diffusion flame operated in both $-g$ and $+g$ configurations to gain an accurate understanding of the gel formation mechanism. ANSYS v14 computational package was used for performing the simulations. Aerosol formation in the flames was modeled by a comprehensive approach as described by Brooks and Moss,[16] which includes terms for carbon NP nucleation, surface growth, coagulation, and oxidation. Our numerical model solves the time-dependent, two-dimensional equations for conservation of mass density, momentum, energy, individual species concentration, f_v and t_{res} distribution inside the FAR, and rates of reaction. The computational grid included the full burner geometry including the extension tube, located downstream of the quartz tube. Acetylene and air flow rates were maintained at 0.65 and 105 l min^{-1}, respectively, for $-g$ and $+g$ configurations, to match our experiments.

Figure 3 shows instantaneous images of axial velocity, t_{res}, and f_v at one time step for our flame system in $-g$ configuration. The "U" shaped stagnation plane of the $-g$ flame is well replicated in our simulation results. The $-g$ flame reaches a maximum axial velocity of 1.5 cm/s, much lesser than the velocity of $+g$ flames under same fuel-air flow conditions. Due to the significant reduction in axial velocity and buoyancy-driven convection in $-g$ flames, diffusion becomes the dominant mechanism of transport.[11] As a result, these flames are much longer and wider than $+g$ flames with thicker diffusion layers.

By tracing the axial velocity vectors in Fig. 3(a), our simulation results suggest that a particle originating at the center of a $-g$ flame gets trapped in a closed-loop recirculation zone, which has a turn-around time of 1.3 s. Under ideal conditions, a trapped particle would be unable to escape and encounters an unlimited t_{res} in this zone. In reality, we observed gravitational forces ejecting gel particles out of the recirculation zone when it grew above ≈1 mm in size.

The area-averaged f_v in the recirculation zone was calculated to be 1×10^{-5}, which is around 100 times greater than

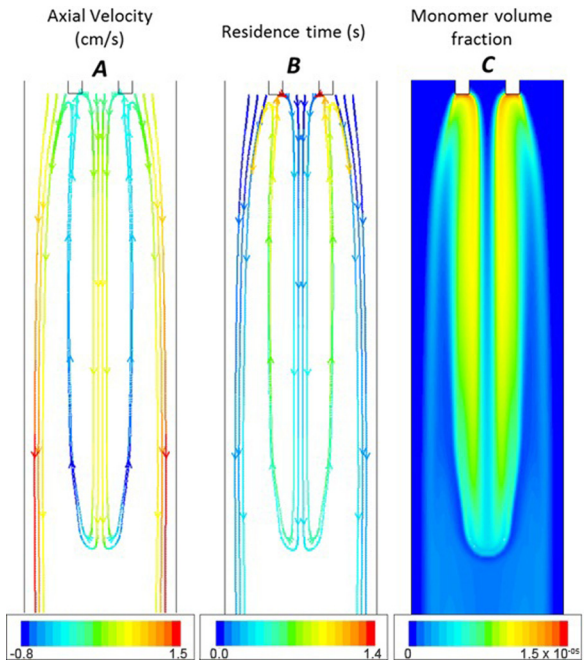

FIG. 3. Two dimensional contour plots of simulated acetylene flame parameters for downward ($-g$) configuration. (a) Particle path lines colored by axial velocity. (b) Path lines colored by particle residence time. (c) Soot monomer volume fraction distribution.

the average f_v (9.8×10^{-8}) in $+g$ flames. Because of the increase in f_v in this zone, the particles emit and absorb larger quantities of thermal radiation. The resulting radiative heat loss causes a decrease in net flame temperature (1900 K), compared to a $+g$ flame (2100 K).

With the knowledge of f_v and a, we estimated the aggregation kernel K in both $-g$ and $+g$ acetylene flames. The average f_v in the recirculation zone can be expressed as

$$f_v = \frac{n\ V_p}{A\ h}, \tag{2}$$

where n is the number of monomers, V_p is the volume of a monomer ($\frac{4}{3}\pi a^3$), A is the view area, and h is the depth of view. For $-g$ flame systems, using Eq. (2), $a = 10 \times 10^{-7}$ cm and $f_v = 1 \times 10^{-5}$, we get $n = 2.4 \times 10^{12}$ cm^{-3}. For $+g$ flame systems, using Eq. (2), $a = 20 \times 10^{-7}$ cm and $f_v = 9 \times 10^{-8}$, we get $n = 2.9 \times 10^9$ cm^{-3}. The growth of DLCA clusters is governed by the Smoluchowski equation,[17] and the mass to linear size (radius of gyration) relationship of the clusters made up of monomers can be expressed as a power-law relationship

$$N = k_0 \left(\frac{R_g}{a}\right)^{D_f}, \tag{3}$$

where N is the number of monomers constituting a cluster, D_f (=1.8 for a cluster-dilute aggregate) is the mass fractal dimension,[17,18] R_g is the aggregate radius of gyration and k_0 is the fractal pre-factor. For millimeter-size aerosol gel clusters, we assumed monodisperse and spherical ($D_f = 3$) clusters as per past recommendation,[9] and calculated their R_g from their perimeter radius R using the equation

$$R_g = \frac{R}{\sqrt{\frac{D_f + 2}{D_f}}}. \quad (4)$$

The average R_g of a gel cluster was calculated to be 0.34 mm. For $+g$ flame-generated sub-micron size clusters, $R_g = L_{max}/3$, where L_{max} is the maximum projected length of a cluster.[19] We calculated the average R_g of $+g$ flame clusters to be 333 nm. For $-g$ flames, using Eq. (3), we calculated average $N = 1.7 \times 10^8$ per aerosol gel cluster. For $+g$ flames, we calculated average $N = 316$ per aggregate. By dividing n by N, we calculated the density of clusters η for $-g$ and $-g$ flames to be 1.36×10^3 and 9.2×10^6 cm^{-3}, respectively. The equation connecting K, aggregation rate kernel, and η is given as[9]

$$K = \frac{d\left(\frac{1}{\eta}\right)}{dt}. \quad (5)$$

We used $t = 0.1$ s, representative of average time for cluster formation in a hydrocarbon flame,[9] and Eq. (5) to calculate K for $-g$ and $+g$ flames to be 7.3×10^{-4} and 1.1×10^{-6} cm^3 s^{-1}, respectively.

Using Eq. (1) and K, we calculated $t_{gel} \approx 60$ ms in the recirculation zone, which is more than eight orders of magnitude lower than $t_{gel} \approx 10^7$ s of a $+g$ flame. This factor of $>10^8$ decrease in t_{gel} coupled with the zone's non-converging t_{res} facilitates the continuous structural arrest of NPs to form gel clusters. We speculate that this zone represents a deep local minimum in the energy landscape.[20] However, verifying this is beyond the scope of this study and a topic of future research.

In conclusion, we demonstrated a facile, high-throughput (grams per hour) carbon aerogel synthesis method via the flame aerosol route. It overcomes the complexities involved in synthesizing carbon aerogels using the non-continuous and time-consuming wet sol-gel process that requires supercritical point drying. Unlike solution phase methods, the flame aerosol route allows better control of the shape and size of monomers.[5] While the SSA of carbon aerogels produced by our technique is lower than those produced via the sol-gel route, past research has shown that particle SSA in flames could be significantly increased by applying external electric fields across the flame flow or by adding additives to the fuel mixture.[21] Our aerogelation mechanism also has the potential of finding applications in the production of advanced functional structures requiring high surface area per unit volume, such as cathode materials for Li-ion batteries[22] and photoactive thin films.[23]

This material is based upon work supported by NASA (Nos. NNX10AR89A and NNX11AB79G), and the Desert Research Institute.

[1]C. J. Brinker and G. W. Scherer, *Sol-Gel Science: The Physics and Chemistry of Sol-Gel Processing* (Elsevier, 1990).
[2]E. J. Lerner, Ind. Phys. **10**(5), 26 (2004).
[3]J. E. Fesmire, Cryogenics **46**(2), 111 (2006).
[4]G. Beaucage, H. K. Kammler, R. Mueller, R. Strobel, N. Agashe, S. E. Pratsinis, and T. Narayanan, Nature Mater. **3**(6), 370 (2004).
[5]S. E. Pratsinis, AIChE J. **56**(12), 3028 (2010).
[6]C. M. Sorensen and A. Chakrabarti, Soft Matter **7**(6), 2284 (2011).
[7]R. Jullien and R. Botet, *Aggregation and Fractal Aggregates* (World Scientific Singapore, 1987).
[8]R. Dhaubhadel, C. S. Gerving, A. Chakrabarti, and C. M. Sorensen, Aerosol Sci. Technol. **41**(8), 804 (2007).
[9]C. M. Sorensen, W. B. Hageman, T. J. Rush, H. Huang, and C. Oh, Phys. Rev. Lett. **80**, 1782 (1998).
[10]R. K. Chakrabarty, H. Moosmüller, M. A. Garro, and C. B. Stipe, Aerosol Sci. Technol. **46**(1), i–iii (2012).
[11]C. R. Kaplan, E. S. Oran, K. Kailasanath, and H. D. Ross, Symp. (Int.) Combust. **26**, 1301 (1996).
[12]D. B. Olson, J. C. Pickens, and R. J. Gill, Combust. Flame **62**(1), 43 (1985).
[13]R. K. Chakrabarty, H. Moosmüller, W. P. Arnott, M. A. Garro, G. Tian, J. G. Slowik, E. S. Cross, J.-H. Han, P. Davidovits, and T. B. Onasch, Phys. Rev. Lett. **102**(23), 235504 (2009).
[14]See supplementary material at http://dx.doi.org/10.1063/1.4884057 for electron microscopy images.
[15]K. J. Rockne, G. L. Taghon, and D. S. Kosson, Chemosphere **41**(8), 1125 (2000).
[16]S. J. Brookes and J. B. Moss, Combust. Flame **116**(4), 486 (1999).
[17]R. Jullien and R. Botet, *Aggregation and Fractal Aggregates* (World Scientific, Singapore, 1987), p. ix.
[18]C. M. Sorensen, Aerosol Sci. Technol. **35**(2), 648 (2001).
[19]R. K. Chakrabarty, H. Moosmüller, W. P. Arnott, M. A. Garro, J. G. Slowik, E. S. Cross, J.-H. Han, P. Davidovits, T. B. Onasch, and D. R. Worsnop, Appl. Opt. **46**(28), 6990 (2007).
[20]C. P. Royall, S. R. Williams, T. Ohtsuka, and H. Tanaka, Nature Mater. **7**(7), 556 (2008).
[21]H. K. Kammler, L. Mädler, and S. E. Pratsinis, Chem. Eng. Technol. **24**(6), 583 (2001).
[22]X. Zhang, H. Zheng, V. Battaglia, and R. L. Axelbaum, Proc. Combust. Inst. **33**(2), 1867 (2011).
[23]E. Thimsen and P. Biswas, AIChE J. **53**(7), 1727 (2007).